Special Issue

Conductivity and Redox Potentials of Ionic Liquid Trihalogen Monoanions $[X_3]^-$, $[XY_2]^-$, and $[BrF_4]^-$ (X = Cl, Br, I and Y = Cl, Br)

Tyler A. Gully, Patrick Voßnacker, Jonas R. Schmid, Helmut Beckers, and Sebastian Riedel*[a]

The ionic liquid (IL) trihalogen monoanions $[N_{2221}][X_3]^-$ and $[N_{2221}][XY_2]^-$ ($[N_{2221}]^+$ = triethylmethylammonium, X = Cl, Br, I, Y = Cl, Br) were investigated electrochemically via temperature dependent conductance and cyclic voltammetry (CV) measurements. The polyhalogen monoanions were measured both as neat salts and as double salts in 1-butyl-1-methyl-pyrrolidinium trifluoromethane-sulfonate ([BMP][OTf], $[X_3]^-/[XY_2]^-$ 0.5 M). Lighter IL trihalogen monoanions displayed higher conductivities than their heavier homologues, with $[Cl_3]^-$ being 1.1 and 3.7 times greater than $[Br_3]^-$ and $[I_3]^-$, respectively. The addition of [BMP][OTf] reduced the conductivity significantly. Within the group of polyhalogen monoanions, the oxidation potential develops in the series $[Cl_3]^- > [BrCl_2]^- > [Br_3]^- > [IBr_2]^- > [ICl_2]^- > [I_3]^-$. The redox potential of the interhalogen monoanions was found to be primarily determined by the central halogen, I in $[ICl_2]^-$ and $[IBr_2]^-$, and Br in $[BrCl_2]^-$. Additionally, tetrafluorobromate(III) ($[N_{2221}]^+[BrF_4]^-$) was analyzed via CV in MeCN at 0 °C, yielding a single reversible redox process ($[BrF_2]^-/[BrF_4]^-$).

1. Introduction

In 1923 Chattaway and Hoyle performed the first thorough characterization of polybromides and polychlorides monoanions.[1] Since then, the trihalogen monoanions of the general form $[X_3]^-$[2,3,4] and $[XY_2]^-$[4–9] (X = Cl, Br, I, Y = F, Cl, Br, and I) have been extensively studied, and higher polyhalogen monoanions such as $[Cl_{13}]^-$[10] or $[Cl(BrCl)_6]^-$[11] have become well established. Amongst the existing interhalogen monoanions two classifications exist, the classical and non-classical variety.[12] Classical interhalogens have a more electropositive center being surrounded by electronegative halogen atoms as found in $[ICl_2]^-$.[9,13] In comparison, in non-classical interhalogens an electronegative center is surrounded by more electropositive dihalogen molecules such as in $[Cl(I_2)_4]^-$, or $[ClI_2]^-$.[9,14] Another point of comparison between the homonuclear $[X_3]^-$ and interhalogen monoanions $[XY_2]^-$ is the solution equilibrium. Due to the variety in halogen atoms, a more complex equilibrium in solution for $[XY_2]^-$ exists compared to that of the homonuclear species.[15–18]

In the solid state, polyhalogens of type $[Br_x]^-$[19] or $[Cl_x]^-$[20] (x = 3–5) are known to form network structures joined by halogen bonds through a so-called sigma-hole.[11] The sigma hole is a region of greater electron density and more positive electrostatic potential located perpendicular to the bonding axis. The use of halogen bonding can be extended to hybrid polyhalogen-halometalate networks. Whereby halometalates, such as $[SbBr_6]^{2-}$,[21] $[BiBr_5]^{2-}$,[22] or $[TeBr_6]^{2-}$[23] are coordinated via $[Br_3]^-$ or Br_2 units. Additionally, interhalogen networks can form between $[TeCl_6]^{2-}$ and Br_2.[24]

The recent advancements in the polyhalogen monoanion structural characterization were due to stabilization of the anion in the solid state by using more bulky organic cations such as $[NR_4]^+$ (R = methyl, ethyl, propyl)[25] $[PPh_2Cl_2]^+$,[2] or $[HMIM]^+$ (1-methyl-1-hexylimadazolium).[26] As a consequence of using these cations to stabilize the polyhalogen anions, ionic liquids (IL) and sometimes room temperature ionic liquids (RT-IL) were formed.[20,26,27] In addition to forming larger polyhalogen monoanions, their conductivity, melting points, and electrochemical properties can be selectively tuned by variation of the cation.[25,28,29] Some typical cations in IL synthesis are the imidazolium,[26,29–31] pyrrolidinium,[31] and alkyl ammonium[27,31] cations, for a list of ions depicted in this work see Scheme 1.

Within the last 10 years a variety of uses concerning polyhalogens were established. For instance, the interhalogen anion in the non-classical salt $[N_{2221}][Cl(BrCl)_2]$ ($[N_{2221}]^+$ = triethylmethyl-ammonium) acts as a halogenating reagent towards alkenes, alkynes, and Michael systems.[32] It was demonstrated that by using $[N_{2221}]^+Cl^-$ gaseous Cl_2 could be sequestered in the salt as a liquid, making it safer and easier to use in the laboratory as a chlorinating agent compared to Cl_2.[27] Very recently, the bonding situation of symmetrical and asymmetrical $[Cl_3]^-$ has been investigated by experimental and computed electron density experiments.[33] In the case of liquid

[a] T. A. Gully, P. Voßnacker, J. R. Schmid, H. Beckers, Prof. Dr. S. Riedel
Freie Universität Berlin
Fachbereich Biologie, Chemie, Pharmazie
Institut für Chemie und Biochemie – Anorganische Chemie
Fabeckstr. 34/36
14195 Berlin (Germany)
E-mail: s.riedel@fu-berlin.de

Supporting information for this article is available on the WWW under https://doi.org/10.1002/open.202000263

Special Issue An invited contribution to a Special Issue dedicated to Material Synthesis in Ionic Liquids.

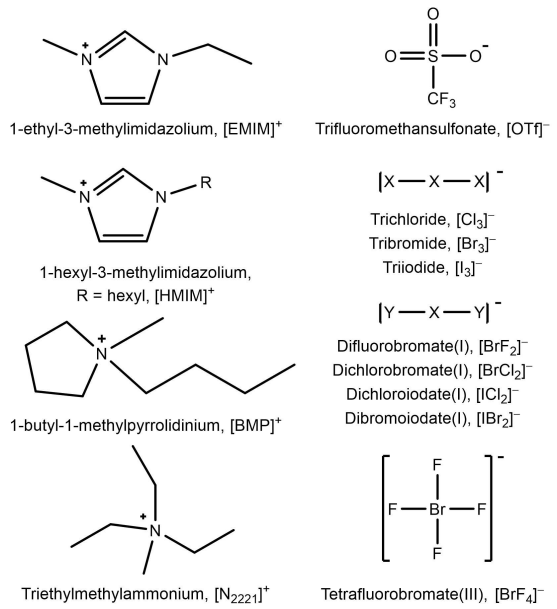

Scheme 1. List of cations and anions used in this work.

Br_2, a solid, $[NBu_4][Br_3]$ or $[NPr_3][Br_9]$,[34] was synthesized to directly perform halogenation reactions.

A significant portion of modern polyhalogen IL applications are based around their electrochemistry, primarily battery technologies. The primary examples are the zinc bromide battery[35,36] and in dye sensitized solar cells.[37,38] In the zinc bromide battery, the purpose of $[Cat]^+Br^-/[Br_3]^-$ is to react with Br_2 and form higher order polyhalogen monoanions that will not gas out of the cell, and as an added benefit increase the conductivity of the electrolyte.[35,36] In dye sensitized solar cells, $[Cat][I_3]$ monoanions act as charge transfer agents.[37,38]

The use of polyhalogens in batteries as charge carriers can be related to their conductance and relationship to the Grotthuss mechanism.[37,39,40] The Grotthuss-like hopping mechanism shuttles X^- moieties within the polyhalogens enabling higher conductivity values in contrast to traditional diffusion based ion transport.[16,38,39,41–43]

The reactive IL can also be further used for the dissolution of UO_2 in $[Cl_3]^-$,[44] recycling of nickel hydride batteries,[45] and the dissolution of rare metals such as Au[11,46,47], Ga,[48] or magnets made of Sm[49] with $[Cl_3]^-$ and $[Br_3]^-$ ILs. Whereby, the determination of the polyhalogen standard potentials could lead to an expedited screening process of determining which metals could be selectively dissolved or chemicals that are readily oxidized into their respective halogenation product.

The electrochemistry of the trihalogen monoanions in non-aqueous media was well studied by Popov in 1958, who did experiments to determine the electrochemical mechanisms of $[I_3]^-$,[50] $[Br_3]^-$[51] and $[ICl_2]^-$[51] and $[IBr_2]^-$[51] in acetonitrile (MeCN) solutions. The other trihalogen monoanions have since been thoroughly characterized in a variety of solvents.[16,18,30,40,52–54] The electrochemistry of molten halogen anions is limited to GaI/$[ICl_2]$, which was investigated at 300 °C.[53]

Bentley *et al.* reexamined the redox chemistry of trihalogen monoanions ILs as double salt ionic liquids (DSIL) via cyclic voltammetry (CV).[15,30] Their purpose was to describe how traces of I^- in ILs were able to etch and dissolve gold electrode surfaces by providing the potentials and redox mechanism of $[I_3]^-$ IL monoanions.[30] By using 1-ethyl-1-methyl-imadazolium bis(trifluoromethanesulfonyl)imide, $[EMIM][NTf_2]$, or trifluoromethanesulfonate, $[OTf]^-$, in combination with the iodide polyhalogens, DSIL salts were formed and studied via CV. The redox mechanism and potential of $[I_3]^-$, and the classical and non-classical interhalogen monoanions, $[ICl_2]^-$ and $[ClI_2]^-$, respectively, were determined.[30]

Subsequently, Bard proposed an electrochemical (E) chemical (C) style mechanism as an ECEC mechanism for the two step oxidation of $Br^-/[Br_3]^-/Br_2$ in nitrobenzene.[55] The mechanism is contrary to previously postulated mechanisms of Allen et al. for Br^-,[56,57] Yu et al. for Br^- and Cl^-,[58] or Bentley et al. for I^-,[30] who propose a CECE style mechanism with the initial step being dependent on the dissociation of X^- and X_2 to $[X_3]^-$. The downside to modeling the CECE mechanism being the high stability of the trihalide monoanion ($K_{eq} > 10^6$ M^{-1}).[30]

Here we present a systematic approach to the electrochemical characterization via conductance and CV measurements of the trihalogen monoanion ILs based on $[N_{2221}][X_3]$ (X = Cl, Br, and I) and classical interhalogen monoanions $[N_{2221}][XY_2]$, (X,Y = Cl, Br, and I) both as neat salts and as DSILs using [BMP][OTf] ($[BMP]^+$ = 1-bu-1-methyl-pyrrolidinium) and [EMIM][OTf] ($[EMIM]^+$ = 1-ethyl-3-methylimidazolium) supporting electrolytes, see Scheme 1. Additionally, the stable interhalogen monoanion $[BrF_4]^-$[5] was characterized via CV in MeCN at 0 °C.

2. Results and Discussion

The homonuclear $[N_{2221}][X_3]$ (X = Cl, Br, and I) and heteronuclear trihalogen monoanions $[N_{2221}][X_3]$ (X = Cl, Br, and I) were synthesized, and their composition confirmed by Raman spectroscopy (see supporting information). The trihalogen monoanion salts display a variety of colors, ranging from yellow $[Cl_3]^-$, yellow-orange $[BrCl_2]^-$, red $[Br_3]^-$, bright red $[IBr_2]^-$, to dark brown-red $[ICl_2]^-$ and dark brown $[I_3]^-$, as shown in Figure 1. The addition of [BMP][OTf] to the neat compounds results in the formation of a DSIL that is liquid at room temperature, yielding an optimal system for electrochemical measurements.

All compounds were analyzed by means of UV-visible spectroscopy (Figure 2), which can also be employed for reaction monitoring. The use of the UV-*vis* spectra as an identifier for chemical reactions will be useful and described in a later section studying the chemical oxidation of metallocenes. A shift in the absorption wavelengths to higher wavelengths is noticeable for the $[X_3]^-$ monoanions from $[Cl_3]^-$ (407 nm), via $[Br_3]^-$ (440 nm), to $[I_3]^-$ (492, 558 nm), whereas the interhalogen monoanions ($[XY_2]^-$) have similar absorptions ranging around 400 nm.

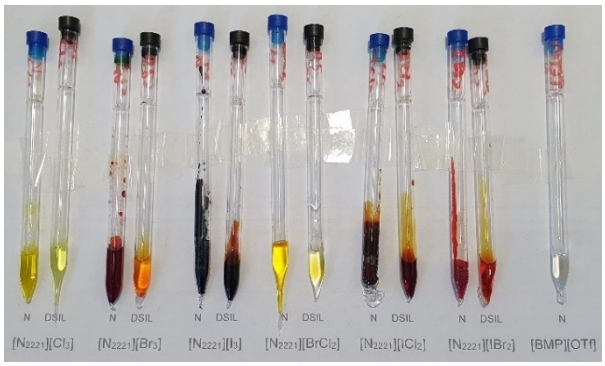

Figure 1. $[N_{2221}][X_3]$ and $[N_{2221}][XY_2]$ as neat liquid (N, left) and mixed with [BMP][OTf] (DSIL, right) ($[X_3]^-$ and $[XY_2]^-$ 0.5 M). The samples from left to right: $[Cl_3]^-$, $[Br_3]^-$, $[I_3]^-$, $[BrCl_2]^-$, $[ICl_2]^-$, $[IBr_2]^-$, $[Cl_3]^-$, [BMP][OTf].

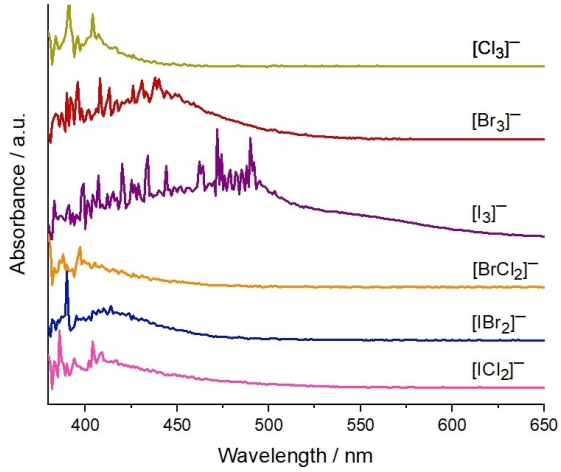

Figure 2. UV-*vis* of $[N_{2221}][X_3]$ and $[N_{2221}][XY_2]$ (X, Y = Cl, Br, I) in MeCN.

2.1. Conductivity

The comparison of physicochemical characteristics, conductivity and viscosity between different ionic liquids is well established in the literature. Polyhalogen anions, however, have relatively large conductivities that are attributable to a Grotthuss-like hopping mechanism.[16,38,39,41–43] Grossi proposed a mechanism based on $[I_3]^-$ in the solid structure. Two $[X_3]^-$ moieties come into contact forming a temporary $[X_6]^-$ molecule ($X_2\cdots X^-\cdots X_3^-$) and subsequently eject a X^- that "hops" to the next $[X_3]^-$ moiety.[16] Based upon their calculations, the insertion of the X^- and the resulting conductivity is heavily dependent on the angle of the incoming $[X_3]^-$ moiety.[16] However, the actual situation in a polyhalogen ILs relating to the Grotthuss-like mechanism are dependent on a variety of other factors including the direction of the mutual intermolecular attack,[16] solvent sheath,[41,42] Coulombic interactions,[59] charge transport,[38,41] diffusion phenomena,[39,43] and halogen dissociation energies.[60]

The temperature dependent conductivity of ILs and DSILs can be modelled by the semi-empirical Vogel-Fulcher-Tamman equation (VFT).[59] The following equation describes the conductivity based VFT equation:

$$\sigma(T) = \sigma_0 exp\left(-\frac{B}{(T - T_g)}\right) \quad (1)$$

Where σ is the conductivity at a given temperature, σ_0 is the conductivity at infinite temperature, B is the thermodynamic probability of particles to interact with each other, and T_g is the glassy transition temperatures. The VFT describes ILs and is valid in IL mixtures of salts and solvents.[59]

$[N_{2221}][Cl_3]^-$ is the only room temperature IL. The other trihalogen monoanions were solid at room temperature, part liquid and solid ($[N_{2221}][Br_3]$), or at the glassy transition phase ($[N_{2221}][BrCl_2]$). The mixture of liquid and solid occurred for $[N_{2221}][IBr_2]$ and $[N_{2221}][ICl_2]$ during the melting process and only the conductivities obtained from a homogeneous melt are presented.

The temperature dependent conductivity of the neat $[N_{2221}][X_3]$ display a clear trend with the lighter halogens having greater conductivity than their heavier homologues ($[Cl_3]^- > [Br_3]^- > [I_3]^-$). Interestingly, $[N_{2221}][Cl_3]$ (44.8 $mS\cdot cm^{-1}$) and $[N_{2221}][Br_3]$ (39.5 $mS\cdot cm^{-1}$) were significantly closer than that of $[N_{2221}][I_3]$ (12.0 $mS\cdot cm^{-1}$) at 55.0 °C, see Figure 3.

In comparison to the $[N_{2221}][X_3]$ salts, the $[N_{2221}][XY_2]$ salts have conductivities that were lower than the conductivity of $[N_{2221}][Br_3]$ but larger than those of $[N_{2221}][I_3]$. The most conductive interhalogen salt contains $[BrCl_2]^-$ (46.5 $mS\cdot cm^{-1}$), followed by $[IBr_2]^-$ (32.4 $mS\cdot cm^{-1}$) and $[ICl_2]^-$ (28.5 $mS\cdot cm^{-1}$). In the range of 70–75 °C, the conductivity of $[ICl_2]^-$ becomes larger than $[IBr_2]^-$, see Table 1.

The addition of the second salt [BMP][OTf] reduced the conductivity of trihalogen monoanions to values similar to [BMP][OTf] compared to their neat salt counterparts, see Figure 4. The [BMP][OTf] will interact with $[N_{2221}][X_3]$ through increased Coulombic interactions caused by the mixing of two

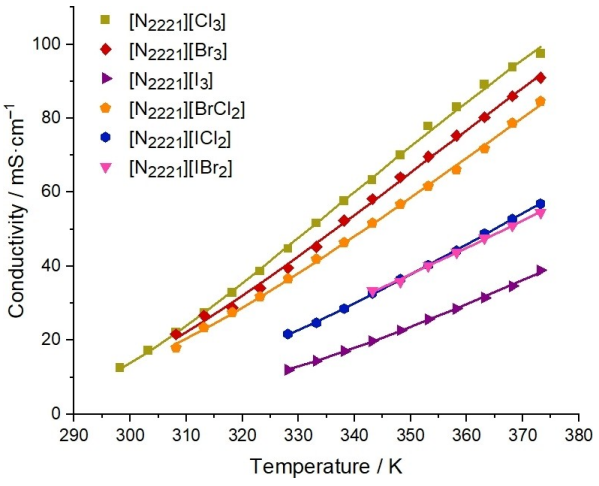

Figure 3. Temperature dependent conductivity of neat $[N_{2221}][X_3]$ and $[N_{2221}][XY_2]$ salts (X,Y = Cl, Br, and I).

Table 1. Conductivity of neat $[N_{2221}][X_3]$ and $[N_{2221}][XY_2]$ (X, Y = Cl, Br, and I) ILs and DSILs in [BMP][OTf] ($[X_3]^-/[XY_2]^-$, 0.5 M) at select temperatures.

Compound	Ionic Liquid	T [°C] and σ [mS·cm^{-1}] 25.0 °C	65.0 °C	100.0 °C
$[Cl_3]^-$	Neat	12.5	57.6	97.5
	[BMP][OTf]	2.5	15.5	34.5
$[Br_3]^-$	Neat	–	52.4	91.0
	[BMP][OTf]	2.2	12.5	29.4
$[I_3]^-$	Neat	–	17.0	38.9
	[BMP][OTf]	1.5	8.2	19.1
$[BrCl_2]^-$	Neat	–	46.5	84.6
	[BMP][OTf]	2.1	13.1	30.2
$[ICl_2]^-$	Neat	–	28.5	56.9
	[BMP][OTf]	2.4	12.4	27.4
$[IBr_2]^-$	Neat	–	32.4	54.6
	[BMP][OTf]	2.3	13.2	28.1
[BMP][OTf]	Neat	1.6	12.2	28.1

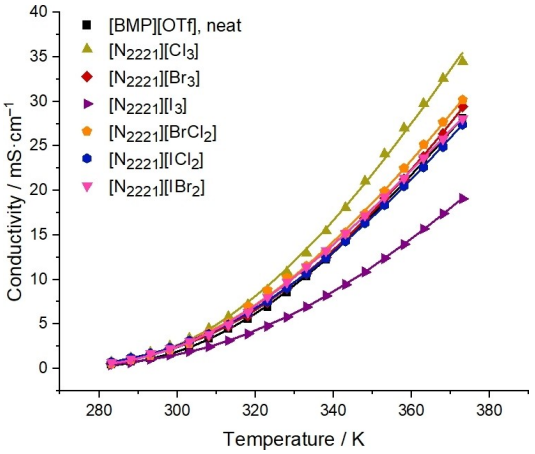

Figure 4. Temperature dependent conductivity of the DSILs $[N_{2221}][X_3]$ and $[N_{2221}][XY_2]$ (X, Y = Cl, Br, I) mixed with [BMP][OTf] ($[X_3]^-/[XY_2]^-$ 0.5 M). [BMP][OTf] is overlapped by the interhalogen monoanions.

ILs,[61] which lead to significantly reduced conductivities in the trihalogen monoanion salts.

The conductivity of the $[X_3]^-$ salts have the same conductivity trends as in the neat trihalogen monoanion ILs. At 25.0 °C, $[Cl_3]^-$ (2.5 mS·cm^{-1}) had the largest conductivity followed by $[Br_3]^-$ (2.2 mS·cm^{-1}) and $[I_3]^-$ (1.5 mS·cm^{-1}), which mirrors the neat $[X_3]^-$ ILs.

By increasing the temperature, the order of the most conductive trihalogen monoanion salts changes. Initially, at T = 25.0 °C, the conductivities are greatest as follows: $[Cl_3]^- > [ICl_2]^- > [IBr_2]^- > [Br_3]^- > [BrCl_2]^- >$ [BMP][OTf] $> [I_3]^-$. In comparison, at higher temperatures, T = 100.0 °C, the order changes slightly: $[Cl_3]^- > [BrCl_2]^- > [Br_3]^- > [IBr_2]^-$ = [BMP][OTf] $> [ICl_2]^- > [I_3]^-$.

2.2. Cyclic Voltammetry

To examine the redox behavior of the trihalogen monoanions under conditions reflecting their use for further applications[32,46] the neat ILs as well as DSILs were investigated.

The cyclic voltammograms of the neat $[Cl_3]^-$, $[Br_3]^-$, and $[I_3]^-$ ILs exhibit under anodic conditions relative to open circuit two redox processes, see Figure 5. We assign the first I, which either occurs as a wave (Br) or a shoulder (Cl, I), to the oxidation of X^- (Eq. 3) being in equilibrium with $[X_3]^-$ (Eq. 2). The second II appears as a current increase denoting the anodic end of the electrochemical window of the respective IL; we assign it to the oxidation of $[X_3]^-$ to X_2 (Eq. 4). This is in accordance to the processes, which have been thoroughly studied in a variety of solvents for X^-, and is observed in Cl^-, Br^-, and I^-:[16,18,30,40,51–53,62]

$$[X_3]^- \rightleftharpoons X^- + X_2 \quad (2)$$

$$3\,X^- \longrightarrow [X_3]^- + 2\,e^- \quad (3)$$

$$[X_3]^- \longrightarrow 1.5\,X_2 + e^- \quad (4)$$

The $E_{1/2}$ potential for the redox process I is given as the following approximation:

$$E_{1/2} = E_{c,p} + \frac{E_{a,p} - E_{c,p}}{2} \quad (5)$$

where $E_{c,p}$ and $E_{a,p}$ are the peak or shoulder (inflection point) potentials of the cathodic and anodic waves. In the Figures 5–9, $E_{c,p}$ and $E_{a,p}$ are displayed as their respective wave, I_c or I_a, respectively. The potential of the redox process II was set at 85 % of current relative to the baseline current of process I. This potential clearly is not comparable to $E_{1/2}$ values, for this reason we call this value E_{II}. The potentials of the redox processes are summarized in Table 2.

Due to the highly concentrated nature of the neat ILs, the observed potentials vary compared to the CVs in nonaqueous solvents,[30,50,51,55] or in other IL salt electrolyte solutions,[30,56] as discussed below.

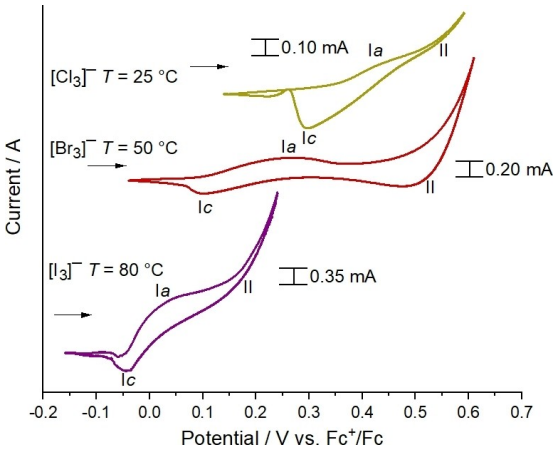

Figure 5. Cyclic voltammograms of neat $[N_{2221}][X_3]$ (X = Cl, Br, I). Scan rate of 10 mV·s^{-1}; the arrow represents scan direction and the zero current; second cycle.

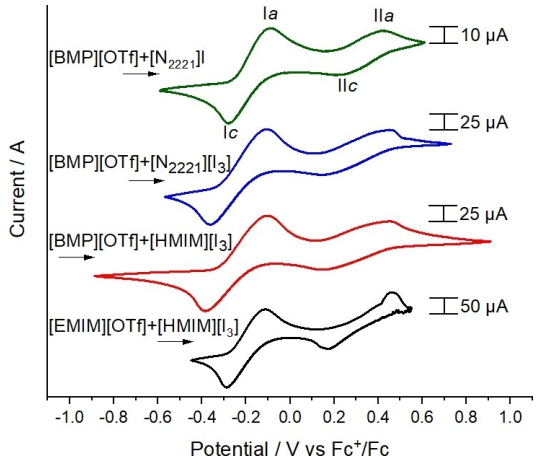

Figure 6. Cyclic voltammograms of [HMIM][I_3] in [EMIM][OTf] ([I_3]$^-$ 0.3 M), in [BMP][OTf] ([I_3]$^-$ 0.34 M), and [N_{2221}][I_3] (0.5 M) and [N_{2221}]I (0.5 M) in [BMP][OTf]. Scan rate of 10 mV·s^{-1}; the arrow represents scan direction and the zero current, second cycle.

Cyclic Voltammetry of DSIL [N_{2221}]$^+$[X_3]$^-$/[XY_2]$^-$ in [BMP][OTf]:

Recently, Bentley et al. had determined the standard potentials of [I_3]$^-$ and [ICl_2]$^-$ in a variety of ILs, specifically [EMIM][I_3] in [EMP][OTf].[15,30] The [EMIM]$^+$ cation is stable in combination with the [I_3]$^-$ monoanion, whereas the [Cl_3]$^-$ monoanion was found to chlorinate the alkyl chains of such cations due to a higher oxidation potential.[20]

Therefore, the [N_{2221}]$^+$ cation and supporting electrolyte [BMP][OTf] was used to determine the trihalogen monoanion potentials. A comparison of the CV results between the imidazolium class cation [HMIM]$^+$ and [N_{2221}]$^+$ with I$^-$ and the [I_3]$^-$ monoanion in the supporting electrolytes [EMIM]$^+$/[BMP]$^+$[OTf]$^-$ is shown in Figure 6.

Starting from the imidazolium salt [HMIM][I_3] in [EMIM][OTf] two redox processes belonging to the I$^-$/[I_3]$^-$ (I, −0.20 V) and [I_3]$^-$/I_2 (II, 0.24 V) were observed and the curve characteristic is comparable to previous studies.[30] [HMIM][I_3] in [BMP][OTf] and [N_{2221}][I_3] also have similar redox potentials varying up to 0.04 V.

The CV of [N_{2221}]I in [BMP][OTf] indicates due to its similarity to that of [N_{2221}][I_3] in [BMP][OTf] two issues. First, the equilibrium between [I_3]$^-$ and I$^-$ + I_2 according to Eq. 2. Second, the dependence of the I-content in the solution on the curve shape. The peaks of both waves Ia and Ic as well as IIa and IIc is by about 0.1 V more separated in case of solutions containing more I ([I_3]$^-$).

With regards to the two wave mechanism of X$^-$/[X_3]$^-$/X_2, two complete mechanisms have been proposed recently, a 4 step CECE mechanism from Bentley et al. (X = I)[30] and an 11 step ECEC mechanism from Bard et al. (X = Br).[55] The proposed mechanisms of Bard and Bentley were simulated to the CV of [N_{2221}][I_3] in [BMP][OTf]. However, while the resulting simulated curves were similar in shape, the simulations were not detailed enough to form a sufficient statement about the mechanism. The rather high concentration of the electrolyte solution or of the neat substance likely, make the measurement unfeasible.

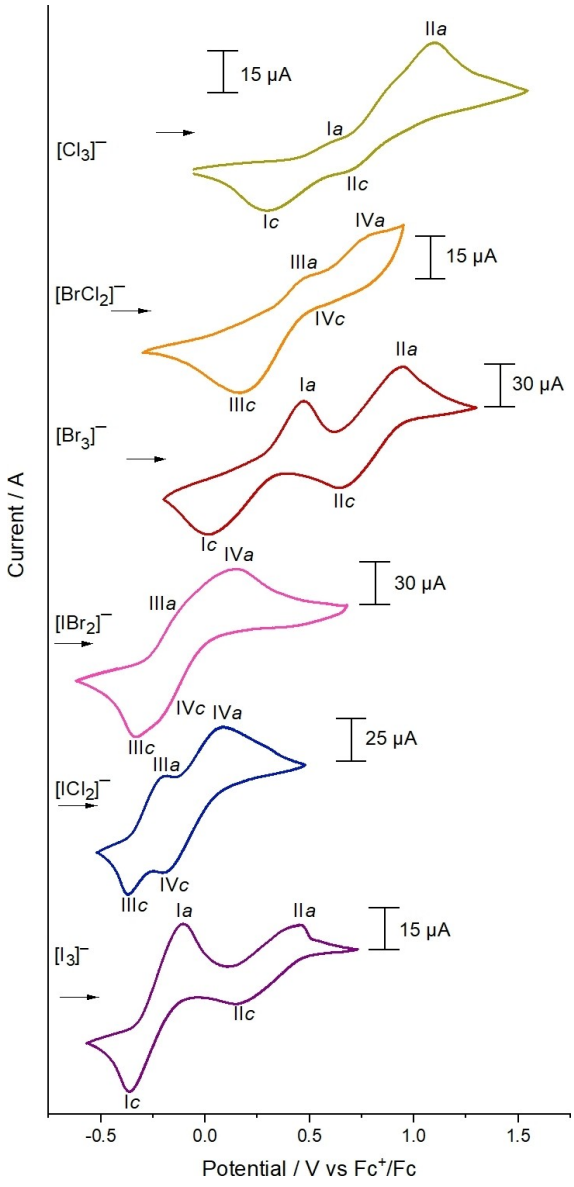

Figure 7. Cyclic voltammograms of [N_{2221}][X_3] and [N_{2221}][XY_2] (X, Y = Cl, Br, I) in [BMP][OTf] ([X_3]$^-$/[XY_2]$^-$ 0.5 M). Scan rate of 10 mV·s^{-1}; the arrow represents scan direction and the zero current, second cycle.

Table 2. The redox potentials of neat [N_{2221}][X_3] (X = Cl, Br, I). Explanations see text.

Ionic Liquid	Temperature [°C]	$E_{1/2}$ or E_{II} (V vs Fc$^+$/Fc) **I** (X$^-$/[X_3]$^-$)	**II** ([X_3]$^-$/X_2)
[N_{2221}][Cl_3]	25	0.37	0.55
[N_{2221}][Br_3]	50	0.18	0.52
[N_{2221}][I_3]	80	−0.02	0.18

Therefore, in this work, only the general mechanism that has been agreed upon in literature[30,56,58] and presented in Eq. 3 and 4 are presented. The focus will be placed on the oxidative power of the concentrates [X_3]$^-$ species in the [BMP][OTf] IL electrolyte solution.

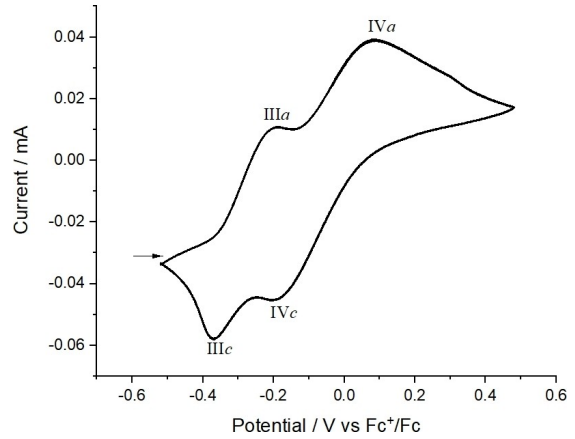

Figure 8. Cyclic voltammogram of $[N_{2221}][ICl_2]$ in [BMP][OTf] ($[ICl_2]^-$ 0.5 M). Scan rate of 10 mV·s^{-1}; the arrow represents scan direction, second cycle.

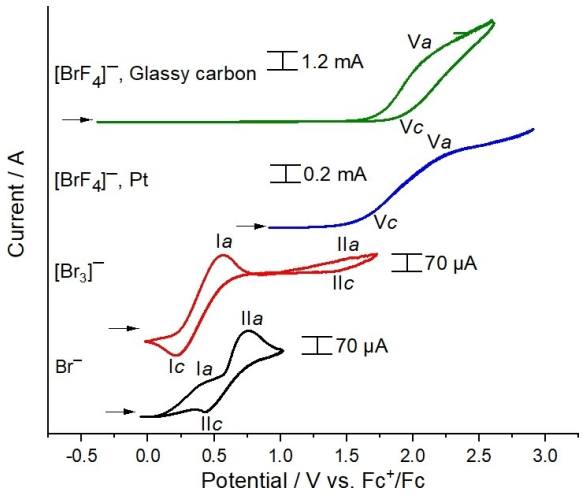

Figure 9. Cyclic voltammogram of $[N_{2221}]^+Br^-/[Br_3]^-/[BrF_4]^-$ (50 mM) in MeCN. The working electrodes are a planar Pt electrode (1 mm diameter) and a planar glassy carbon electrode (2 mm diameter) Measured at a temperature of 0 °C; scan rate of 100 mV s^{-}; and the arrow represents scan direction and the zero current, second cycle.

Due to $[N_{2221}][I_3]$ in [BMP][OTf] displaying similar redox potentials independent of the cation and the supporting electrolyte, the cation $[N_{2221}]^+$ and the supporting electrolyte [BMP][OTf] will be used for the other trihalogen monoanions.

Based upon the trihalogen monoanion, the redox potential for wave **I** varies significantly. The strongest oxidizing agent, based on $X^-/[X_3]^-$, being $[Cl_3]^-$ (0.46 V) followed by $[Br_3]^-$ (0.25 V) then $[I_3]^-$ (−0.24 V) (Figure 7, Table 3).

For $[Cl_3]^-$ two observable oxidation steps for the $[Cl_3]^-/Cl_2$ occurred for the scan rate of 10 mV·s^{-1}. The initial shoulder at 0.86 V disappears at scan rates of 1000 m V·s^{-1} (Figure S23). The resulting shoulder at 0.86 V likely results due to the influence of the redox couples **I** and **II** on each other. The calculated $E_{1/2}$ value for wave **II** of $[Cl_3]^-$ should therefore be used with caution.

The interhalogen monoanions have differing electrochemistry compared to $[X_3]^-$, as seen in the CVs of $[ICl_2]^-$, $[IBr_2]^-$, and

Table 3. The $E_{1/2}$ redox potentials of DSILs $[Cat][X_3]$ and $[Cat][XY_2]$ (X and Y = Cl, Br, I) in [BMP][OTf] or [EMP][OTf] ($[X_3]^-/[XY_2]^-$ 0.5 M).

Ionic Liquid	Additive Salt	$E_{1/2}$ (V vs Fc^+/Fc) **I** ($X^-/[X_3]^-$)	**II** ($[X_3]^-/X_2$)
$[N_{2221}][Cl_3]$	[BMP][OTf]	0.46	0.90
$[N_{2221}][Br_3]$	[BMP][OTf]	0.25	0.81
$[N_{2221}][I_3]$	[BMP][OTf]	−0.24	0.31
$[N_{2221}]I$	[BMP][OTf]	−0.18	0.33
$[HMIM][I_3]^a$	[BMP][OTf]	−0.24	0.31
$[HMIM][I_3]^b$	[EMIM][OTf]	−0.20	0.32
		III ($X^-/[X_3]^-$)	**IV** ($[ICl_2]^-/ICl_3 + [Cl(ICl)_2]^-$)
$[N_{2221}][BrCl_2]$	[BMP][OTf]	0.33	0.70
$[N_{2221}][IBr_2]$	[BMP][OTf]	−0.24	−0.02
$[N_{2221}][ICl_2]$	[BMP][OTf]	−0.28	−0.05

[a] $[I_3]^-$ 0.34 M, [b] $[I_3]^-$ 0.3 M

$[BrCl_2]^-$. $[ICl_2]^-$ in [BMP][OTf] has 2 different quasi-irreversible redox processes, see Figure 8. The liquid phase equilibrium of interhalogen monoanions and the electrochemical products concerning them has been continually investigated since Popov in 1958.[15,17,51,63] A recently reported mechanism for the electrochemical oxidation of the I^- and Cl^- in $[EMIM]^+$ bis (trifluoromethanesulfonyl)imide consists of a combination of electrochemical-chemical (EC) mechanisms and the production of several interhalogen monoanion species.[15,30]

Despite, $[ICl_2]^-$ being a molecule composed of two halogens, the possible resulting mixtures due to the various chemical rearrangements and electron transfer reactions lead to a complex mechanism. Since the variety of synthesized interhalogens of type XY, XY_3, XY_5, or $[X_aY_b]^-$ (a = 1–5, b = 2–6)[13,64] is rather large and the determination of the mechanism becomes complicated. Therefore, in the present work, we postulate a simplified mechanism for the interhalogens of type $[XY_2]^-$. In a future work we will perform Raman spectroelectrochemical measurements to help elucidate the electrochemical mechanism of the $[XY_2]^-$ species.

On the basis of $[XY_2]^-$ two redox processes where observed. The proposed oxidation of III starts with the equilibrium between $[XY_2]^-$ and I^- and Cl^- (Eq. 6) followed by the oxidation of X^- to $[X_3]^-$ (Eq. 7). The reasoning for this oxidation stems from the comparison between trihalogen monoanions. The redox potentials of I are very similar to the shoulder of III, based upon the central halogen atom, see Figure 7. The species $[N_{2221}][I_3]$ for I has a similar potential (−0.24 V) to those of III for $[N_{2221}][ICl_2]$ (−0.28 V) and $[N_{2221}][IBr_2]$ (−0.24 V). This can also be expanded to $[Br_3]^-$ (0.25 V) and $[BrCl_2]^-$ (0.33 V).

$$[XY_2]^- \rightleftharpoons X^- + 2\,Y^- \quad (6)$$

$$3\,X^- \longrightarrow [X_3]^- + 2\,e^- \quad (7)$$

However, the second redox couple of $[ICl_2]^-$ and $[IBr_2]^-$ (IV) differed significantly from $[I_3]^-$ (II).

The subsequent oxidation at IV, is also analogous to $[X_3]^-$, with the oxidation of the trihalide species $[XY_2]^-$ to $[XY_4]^-$ and

X_2 (Eq 8). With the oxidation IV_a of $[XY_2]^-$ occurring at lower potentials than $[X_3]^-$. In the case of $[ICl_2]^-$ and $[IBr_2]^-$ the formation of I_2 at the WE could explain the drop in the anodic current.

$$2\,[XY_2]^- \longrightarrow [XY_4]^- + 0.5\,X_2 + e^- \quad (8)$$

Both CVs of the trihalogen monoanions as neat and DSIL salts were measured and found to undergo the same redox processes, although at slightly differing potentials. The difference in potential between the neat IL and DSIL is caused by difference between electrolyte solution of the trihalogen monoanions. The addition of [BMP][OTf] likely influences the Coulombic interactions between trihalogen monoanions, resulting in shifted potentials from the neat salt to potentials similar to previous reports.[30]

Chemical oxidation of metallocenes with trihalogen monoanions: To determine the oxidation strength of the trihalogen monoanions based upon chemical means, and not to elucidate the electrochemical mechanism, a variety of metallocenes ($TiCp_2Cl_2$, $RuCp_2$, AcFc (acetylferrocene), Fc, $FcCp^*_2$ (decamethylferrocene), and $CoCp_2$) with differing potentials,[65–69] see Table 4, were added to $[N_{2221}][X_3]$ and $[N_{2221}][XY_2]$ (X,Y = Cl, Br, I) in MeCN. The benefit to metallocenes is that the potential is tunable based upon the metal center and the substituents on the cyclopentadienyl ring.[66] Addition of the polyhalogen will act as an oxidizing agent, a one electron process should occur.[68]

A visible color change will be observed, if the diluted (MeCN) trihalogen monoanion oxidizes the metallocene. When no reaction occurred the color remained unchanged. The absorption and change of absorption wavelengths were further examined via UV-*vis* spectroscopy to monitor the metallocene oxidation, see SI Figures S9–15 and Table S1 in the Supporting Information. The following series displays the oxidation power of the investigated trihalogen monoanions, where any trihalogen monoanion will oxidize the species to its left: $CoCp_2 < FcCp^*_2 < Fc < [I_3]^- < [ICl_2]^- < [IBr_2]^- < [Br_3]^- < AcFc < RuCp_2 < [BrCl_2]^- < [Cl_3]^-$.

According to the recorded UV-vis spectra $CoCp_2$, $FcCp^*_2$, and Fc were oxidized by all trihalogen monoanions. Only $[BrCl_2]^-$ and $[Cl_3]^-$ had sufficient oxidation strength to oxidize $RuCp_2$ and AcFc. Lastly, $TiCp_2Cl_2$ did not react with any of the trihalogen monoanions.[69]

The $[ClF_4]^-/[BrF_4]^-/[IF_4]^-$ species are well known structurally,[5–7,70] but the electrochemical characterization is currently lacking in the literature. Therefore, the CVs of $[N_{2221}]Br$ and $[N_{2221}][Br_3]$ were measured under the same conditions (50 mM, MeCN, $T = 0\,^\circ C$) to adequately compare other known bromide monoanions to the redox processes of $[N_{2221}][BrF_4]$, see Figure 9.

The redox processes of Br^- and $[Br_3]^-$ undergo the same redox processes as in the previously described (see Equations 2 and 3). In regards to Br^- for I ($Br^-/[Br_3]^-$), only the anodic wave was visible as a shoulder at 0.40 V. The second wave was irreversible with the anodic II*a* ($[Br_3]^-/Br_2$) occurring at 0.75 V and cathodic wave II*b* at 0.43 V, see Table 5.

The $[Br_3]^-$ species also undergoes the an irreversible reaction from wave **I** ($Br^-/[Br_3]^-$) with a peak separation of 350 mV. The second redox couple ($[Br_3]^-/Br^-$) is only quasi-reversible at 1.47 V. The results for Br^- and $[Br_3]^-$ yielded similar results to Popov and Geske's original study of Br^- and $[Br_3]^-$ in MeCN.[51]

The fluoride based $[BrF_4]^-$ is a strong oxidizing agent and can be used as a brominating agent in organic reactions,[71] and can oxidize Pt to form $[PtF_4]^{2-}$ or $[PtF_6]^{2-}$ at $T > 400\,^\circ C$.[72] Using the Pt WE, a single irreversible redox couple was observed, V. The change in current slope forming two shoulders are denoted as V*c* (1.71 V) and V*a* (2.21 V), and were used to determine the $E_{1/2}$ potential (1.96 V). Based on the CV a first postulate was the oxidation of Pt to $[PtF_4]^{2-}$ or $[PtF_6]^{2-}$. However, upon changing the WE to glassy carbon (GC), the two shoulders V*a* (1.93 V) and V*c* (2.05 V) were measured with similar potentials to the Pt electrode. Therefore, Pt is unlikely oxidized during V, rather a different redox couple exists.

To the redox couple of $[BrF_4]^-$, we postulate two separate mechanisms, one based on a CEC mechanism and the other on an CECC mechanism. Both mechanisms yield BrF_5.

The CEC mechanism starts with the equilibrium between $[BrF_4]^-$ to BrF_3 and F^- (Eq. 9). The dissociation of $[I_3]^-$ and $[Br_3]^-$ have been proposed previously,[30,56,57] and could therefore be applied to the interhalogen $[BrF_4]^-$ mechanism. The second step is the subsequent oxidation of F^- to F_2 (Eq. 10) at 2.21 V (Va) at the Pt WE surface. Barrès et al. have demonstrated that the oxidation of F^- to F_2 from $NEt_3 \cdot 3HF$ in MeCN occurs at 2.2 and 3 V vs SCE depending on if the F^- is adsorbed at a Pt electrode or in solution, respectively.[73] The anodic shoulder is at a relatively large potential, so the oxidation to F_2 is possible. The last step is the chemical reaction between F_2 and BrF_3 to BrF_5 (Eq. 11). Gross and Meinert have demonstrated that BrF_5 is stable in acetonitrile,[74] thus the end product seems possible.

$$[BrF_4]^- \rightleftharpoons BrF_3 + F^- \quad (9)$$

Table 4. Redox potentials of various metallocenes (V vs Fc).

Half-reaction	Electrolyte solution	$E^{o\prime}$ [V]
$RuCp_2 \rightleftharpoons [RuCp_2]^+ + e^-$	CH_2Cl_2/0.05 M $BArF_{24}$	0.56[68]
$RuCp_2 \rightleftharpoons [RuCp_2]^+ + e^-$	CH_2Cl_2/0.1 M TFAB	0.41[68]
$AcFc \rightleftharpoons [AcFc]^+ + e^-$	MeCN	0.26[66,67]
$Fc \rightleftharpoons [Fc]^+ + e^-$	MeCN	0[65]
$FcCp^*_2 \rightleftharpoons [FcCp^*_2]^+ + e^-$	MeCN	−0.59[65]
$TiCp_2Cl + Cl^- \rightleftharpoons TiCp_2Cl_2 + e^-$	THF/0.2 M Bu_4NPF_6	−1.27[69]
$CoCp_2 \rightleftharpoons [CoCp_2]^+ + e^-$	CH_2Cl_2	−1.33[65]

Table 5. The $E_{1/2}$ redox potentials of $[N_{2221}]^+Br^-/[Br_3]^-/[BrF_4]^-$ (50 mM) in MeCN.

Ionic Liquid	Working Electrode	$E_{1/2}$ (V vs Fc^+/Fc) **I** ($Br^-/[Br_3]^-$)	**II** ($[Br_3]^-/Br_2$)	**V** ($[BrF_4]^-/BrF_5$)
$[N_{2221}]Br$	Pt	0.40[a]	0.59	–
$[N_{2221}][Br_3]$	Pt	0.39	1.47	–
$[N_{2221}][BrF_4]$	Pt	–	–	1.96
$[N_{2221}][BrF_4]$	GC	–	–	1.99

[a] $E_{a,p}$

$$2\,F^- \longrightarrow F_2 + 2\,e^- \quad (10)$$

$$F_2 + BrF_3 \longrightarrow BrF_5 \quad (11)$$

The CECC mechanism also starts with the dissociation of $[BrF_4]^-$ to BrF_3 and F^- (Eq. 9) followed by the oxidation of F^- to F_2 (Eq. 10). However the F_2 would subsequently react with $[BrF_4]^-$ to form $[BrF_6]^-$ (Eq. 12). The electrochemically produced species $[BrF_6]^-$ is stable in MeCN when prepared with $[N(CH_3)_4]^+$ F^- and $CsBrF_4$.[5] Thus, the species formation seems logic. The last step is the dissociation of F^- from $[BrF_6]^-$ to form BrF_5 (Eq. 13).

$$F_2 + [BrF_4]^- \longrightarrow [BrF_6]^- \quad (12)$$

$$[BrF_6]^- \rightleftharpoons BrF_5 + F^- \quad (13)$$

The reduction of the newly generated BrF_5 would proceed in reverse of either the proposed mechanisms. Comparing the CVs between the GC and Pt WEs indicates the reduction step occurs independently of the electrode material.

After the CV a ^{19}F NMR was measured and the strongest signal ($\delta = -35.54$ ppm) was assigned to $[BrF_4]^-$, concurring with a previous report.[5]

As an interesting aside, the introduction of Fc to the solution as an external redox couple did not result in the chemical destruction of Fc. Rather, Fc was oxidized to Fc^+ in solution turning a dark blue-green color, forming the salt $[Fc]^+$ $[BrF_4]^-$. Other metallocenes may also form stable ionic compounds with $[BrF_4]^-$.

3. Conclusions

Conductivities and redox potentials of the $[N_{2221}][X_3]$ and $[XY_2]^-$ trihalogen monoanions were determined. The conductivity of the neat salts indicates a clear trend of the respective homologues, with lighter $[Cl_3]^-$ having the largest and heavier $[I_3]^-$ the lowest conductivity. The interhalogen monoanions conductivities of $[ICl_2]^-$, $[IBr_2]^-$, and $[BrCl_2]^-$ were found to range between $[Br_3]^-$ and $[I_3]^-$. The DSIL mixtures with [BMP][OTf] displayed significantly reduced conductivity for all salts. Interestingly, the conductivity measurements of the DSIL salts revealed a different temperature dependence for the trihalogen monoanions. For instance, $[ICl_2]^-$ was more conductive than $[IBr_2]^-$ at 25 °C, but the reverse is true at 100 °C.

The experimental potentials for the neat polyhalogen monoanions were measured via cyclic voltammetry and containing useful information for the oxidation of various compounds. Of the homohalogens $[Cl_3]^-$ is the strongest oxidizing agent followed by $[Br_3]^-$ and $[I_3]^-$. The mechanism regarding the interhalogen system is not well known and a simple mechanism is proposed. However, the mechanism for the interhalogen system is complex due to the formation of various interhalogen compounds. Future work using Raman spectroelectrochemical techniques will be used to further identify the mechanism.

The interhalogen oxidation strength was also compared chemically by reacting the trihalogen monoanions with various metallocenes in acetonitrile. $[Cl_3]^-$ and $[BrCl_2]^-$ were able to oxidize all tested metallocenes, including $RuCp_2$. In comparison, Fc was oxidized by all investigated trihalogen monoanions.

A first look into the electrochemistry of the fluorobromate monoanion, $[BrF_4]^-$, was examined via cyclic voltammetry in acetonitrile. One quasi-reversible redox couple was found, which is proposed to be associated with $[BrF_4]^-/BrF_5$. Two separate mechanisms for the redox couple have been proposed both based on the dissociation of $[BrF_4]^-$ to F^- and subsequent oxidation to F_2. Additionally, the oxidation potential of $[BrF_4]^-$ is significantly greater than that of both $[Br_3]^-$ and Br^-. Based on the proposed redox couple in $[BrF_4]^-$ a similar redox couple could exist in $[ClF_4]^-$ and $[IF_4]^-$.

Experimental Section

Reagents

All experiments were performed using standard Schlenk techniques using argon gas. The following chemicals were purchased [HMIM]I (*Io-li-tec*, 99%), [BMP][OTf] (*Merck*, TH_Geyer CM, 99%), [EMIM][OTf] (*Solvent Innovations*, 99%), $[N_{2221}]Cl$ (*TCI*, 98.0%), $[N_{2221}]Br$ (*Fluorochem*, 95%), Cl_2 (*Linde Gas*, 2.5 purity), Br_2 (*Acros Organics*, 99+%) subsequently condensed onto activated A3 molecular sieves, I_2 (*Riedel-de Haën*, 99.8%), ferrocene (Fc, *Fluorochem*, 99.9%), ruthenocene ($RuCp_2$) (*Abcr*, 99.9%-Ru), acetyl ferrocene (AcFc, *Fluka*, 95% CHN), cobaltecene ($CoCp_2$, *Sigma*), decamethylferrocene (FcCp*2, Sigma, 97%). $[N_{2221}]I$ was prepared according to literature.[75]

Preparation of the trihalogen monoanion ILs occurred by adding (I_2) or condensing (Cl_2, Br_2) one equiv. of X_2 (Cl, Br, or I) to one equiv. of their respective halogen salt $[N_{2221}]X$. To obtain the homogeneous salt ($[N_{2221}][X_3]/[XY_2]$), the mixture was liquified at temperatures not exceeding 120 °C. For exact preparation of the trihalogen monoanion ILs, please see supporting information. The double salt ionic liquid mixtures (DSIL) of [Cat.][X_3] and [Cat.][XY_2] with [BMP][OTf] have a concentration of 0.5 M, except where noted.

UV/Vis and Raman Spectroscopy and Conductivity Methods

The UV-*vis* spectra were recorded using a Perkin Elmer Lambda 465 photometer with deuterium and tungsten lamps. A quartz cuvette with a Rydberg-Schlenk attachment was used to maintain an argon atmosphere. Raman-spectra were measured at −40 °C or *r.t.* using a MultiRAM FT-Raman-Spectrometer by Bruker, equipped with a Nd:YAG-laser and a Ge-detector cooled with liquid nitrogen (1064 nm, 30–450 mW, 64–256 scans, resolution: 2 cm). The temperature dependent conductivity was measured using the *Mettler Toledo AG* SevenCompact S230 Conductivity Meter and INLAB® 710 sensor. Measurements were performed under argon counter flow. The temperature was gradually raised $T = 8$–100 °C in an oil bath.

Electrochemistry

A three electrode configuration and *Bio-Logic* SP-300 potentiostat was used. The working electrode (WE) and counter electrode (CE)

were planar Pt electrodes (1 mm diameter). The electrodes were rinsed with HNO_3, isopropanol, acetone and ethyl acetate. Subsequent Pt electrode activation occurred by polishing with 0.1 μm diamond polish (*Zimmer and Peacock*) rinsed with distilled water followed by 0.05 μm alumina polish (*Zimmer and Peacock*) and rinsed with distilled water. Excess alumina was removed in a sonication bath in distilled water. The electrode was subsequently cycled between the oxygen and hydrogen evolution potentials in 0.1 M H_2SO_4 as described in literature.[76] The Ag reference electrode (RE) was prepared based on literature,[15,30] by taking a Ag wire dipped into the IL or DSIL electrolyte fill solution in a fritted RE (alumina frit, *Ionode*, EChem-Ref-R-SR). The REs were allowed an equilibrium time of 12 h to 5 d, depending on the salt. All experiments were performed under argon. All CVs presented are of the second cycle, as negligible deviation from the first cycle was recorded.

To measure the CVs of neat $[N_{2221}][Br_3]$ and $[N_{2221}][I_3]$ the temperature was raised to 50 °C and 80 °C, respectively, to keep the salt as a melt. The DSILs were all in the liquid phase at room temperature, making the measurement of all trihalogen monoanions feasible.

$[N_{2221}][BrF_4]$ (50 mM) was prepared in MeCN at −40 °C and the cyclic voltammogram (CV) measured at 0 °C. The electrochemical cell was a three electrode set-up with the WE, CE and RE being planar Pt electrodes (1 mm diameter) and a planar glassy carbon WE (2 mm diameter, *HTW*, Sigradur G) coated in perfluoroalkoxy alkanes (PFA). The transfer of solution was performed at −40 °C by placing a PFA tube into the solution and applying a slight overpressure via argon gas. Thus, pumping the liquid into the cell. The cell design and inert transfer of solution to the cell is based on literature.[77]

CV simulations performed using DigiElch-Professional v8.F (ElchSoft.com).

Safety Precautions

Addition of sufficient amounts of Fc to neat $[N_{2221}][Cl_3]$ under Ar is strongly exothermic and produces smoke. If exposed to air, the mixture ignites at *r.t.* Additionally, higher concentrations of $[BrF_4]^-$ than given in this paper can lead to gas evolution of F_2, leading to explosions. At higher concentrations of $[BrF_4]^-$ it probably reacts vigorously upon contact with Fc in a similar fashion to neat $[Cl_3]^-$.

Acknowledgements

We thank the priority program SPP 1708 for financial support and Dr. Valentin Radtke for scientific discourse.

Conflict of Interest

The authors declare no conflict of interest.

Keywords: polyhalogen monoanions · cyclic voltammetry · ionic liquids · conductivit · tetrafluorobromate

[1] F. D. Chattaway, G. Hoyle, *J. Chem. Soc. Trans.* **1923**, *123*, 654.
[2] J. Taraba, Z. Zak, *Inorg. Chem.* **2003**, *42*, 3591.
[3] a) Z. Sun, K. B. Moore, J. G. Hill, K. A. Peterson, H. F. Schaefer, R. Hoffmann, *J. Phys. Chem. B* **2018**, ; b) A. W. Coleman, C. M. Means, S. G. Bott, J. L. Atwood, *J. Crystallogr. Spectrosc. Res.* **1990**, *20*, 199; c) T. Bernstein, F. H. Herbstein, *Acta Crystallogr. B* **1968**, *24*, 1640.
[4] A. I. Popov, in: *Halogen Chemistry* (Ed.: V. Gutmann), Academic Press, New York, **1967**, pp. 225–264.
[5] W. W. Wilson, K. O. Christe, *Inorg. Chem.* **1989**, *28*, 4172.
[6] X. Zhang, K. Seppelt, *Z. Anorg. Allg. Chem.* **1997**, *623*, 491.
[7] S. Ivlev, P. Woidy, V. Sobolev, I. Gerin, R. Ostvald, F. Kraus, *Z. Anorg. Allg. Chem.* **2013**, *639*, 2846.
[8] a) B. S. Ault, L. Andrews, *Inorg. Chem.* **1977**, *16*, 2024; b) G. L. Breneman, R. D. Willett, *Acta Crystallogr.* **1967**, *23*, 334.
[9] L. F. Olsson, *Inorg. Chem.* **1985**, *24*, 1398.
[10] K. Sonnenberg, P. Pröhm, N. Schwarze, C. Müller, H. Beckers, S. Riedel, *Angew. Chem. Int. Ed.* **2018**, *57*, 9136.
[11] B. Schmidt, K. Sonnenberg, H. Beckers, S. Steinhauer, S. Riedel, *Angew. Chem. Int. Ed.* **2018**, *57*, 9141.
[12] H. Haller, S. Riedel, *Z. Anorg. Allg. Chem.* **2014**, *640*, 1281.
[13] R. W. G. Wyckoff, *J. Am. Chem. Soc.* **1920**, *42*, 1100.
[14] Y.-Q. Wang, Z.-M. Wang, C.-S. Liao, C.-H. Yan, *Acta Crystallogr. C* **1999**, *55*, 1503.
[15] C. L. Bentley, A. M. Bond, A. F. Hollenkamp, P. J. Mahon, J. Zhang, *Anal. Chem.* **2016**, *88*, 1915.
[16] J. Grossi, J. J. Kohanoff, N. J. English, E. M. Bringa, M. G. Del Pópolo, *J. Phys. Chem. B* **2017**, *121*, 6436.
[17] T. X. Wang, M. D. Kelley, J. N. Cooper, R. C. Beckwith, D. W. Margerum, *Inorg. Chem.* **1994**, *33*, 5872.
[18] J. Xu, N. S. Georgescu, D. A. Scherson, *J. Electrochem. Soc.* **2014**, *161*, H392–H398.
[19] a) I. D. Gorokh, S. A. Adonin, A. S. Novikov, M. N. Sokolov, D. G. Samsonenko, V. P. Fedin, *J. Mol. Struct.* **2019**, *1179*, 725; b) I. D. Gorokh, S. A. Adonin, M. N. Sokolov, P. A. Abramov, I. V. Korolkov, E. Y. Semitut, V. P. Fedin, *Inorg. Chim. Acta* **2018**, *469*, 583.
[20] R. Brückner, H. Haller, S. Steinhauer, C. Müller, S. Riedel, *Angew. Chem. Int. Ed.* **2015**, *54*, 15579.
[21] a) S. A. Adonin, M. A. Bondarenko, A. S. Novikov, P. A. Abramov, P. E. Plyusnin, M. N. Sokolov, V. P. Fedin, *Z. Anorg. Allg. Chem.* **2019**, *645*, 1141; b) S. A. Adonin, M. A. Bondarenko, A. S. Novikov, P. E. Plyusnin, I. V. Korolkov, M. N. Sokolov, V. P. Fedin, *Inorg. Chim. Acta* **2020**, *502*, 119278; c) S. A. Adonin, M. A. Bondarenko, A. S. Novikov, P. A. Abramov, P. E. Plyusnin, M. N. Sokolov, V. P. Fedin, *CrystEngComm* **2019**, *21*, 850.
[22] S. A. Adonin, I. D. Gorokh, A. S. Novikov, D. G. Samsonenko, P. E. Plyusnin, M. N. Sokolov, V. P. Fedin, *Dalton Trans.* **2018**, *47*, 2683.
[23] A. N. Usoltsev, S. A. Adonin, A. S. Novikov, M. N. Sokolov, V. P. Fedin, *J. Coord. Chem.* **2019**, *72*, 1890.
[24] A. N. Usoltsev, S. A. Adonin, A. S. Novikov, P. A. Abramov, M. N. Sokolov, V. P. Fedin, *CrystEngComm* **2020**, *22*, 1985.
[25] H. Haller, M. Ellwanger, A. Higelin, S. Riedel, *Z. Anorg. Allg. Chem.* **2012**, *638*, 553.
[26] H. Haller, M. Hog, F. Scholz, H. Scherer, I. Krossing, S. Riedel, *Z. Naturforsch.* **2013**, *68b*, 1103.
[27] H. Haller, *Dissertation*, Albert-Ludwigs-Universität Freiburg, Freiburg, **2014**.
[28] a) D. S. Silvester, R. G. Compton, *Z. Phys. Chem.* **2006**, *220*, 1247; b) G. Adamová, R. L. Gardas, M. Nieuwenhuyzen, A. V. Puga, L. P. N. Rebelo, A. J. Robertson, K. R. Seddon, *Dalton Trans.* **2012**, *41*, 8316.
[29] J. S. Wilkes, J. A. Levisky, R. A. Wilson, C. L. Hussey, *Inorg. Chem.* **1982**, *21*, 1263.
[30] C. L. Bentley, A. M. Bond, A. F. Hollenkamp, P. J. Mahon, J. Zhang, *J. Phys. Chem. C* **2015**, *119*, 22392.
[31] S. Zhang, N. Sun, X. He, X. Lu, X. Zhang, *J. Phys. Chem. Ref. Data* **2006**, *35*, 1475.
[32] B. Schmidt, S. Ponath, J. Hannemann, P. Voßnacker, K. Sonnenberg, M. Christmann, S. Riedel, *Chem. Eur. J.* **2020**, *25*, 15183.
[33] H. Keil, K. Sonnenberg, C. Müller, R. Herbst-Irmer, H. Beckers, S. Riedel, D. Stalke, *Angew. Chem. Int. Ed.* **2021**, *60*, 2569, 132, 1.
[34] T. M. Beck, H. Haller, J. Streuff, S. Riedel, *Synthesis* **2014**, *46*, 740.
[35] M. E. Easton, P. Turner, A. F. Masters, T. Maschmeyer, *RSC Adv.* **2015**, *5*, 83674.
[36] M. Schneider, G. P. Rajarathnam, M. E. Easton, A. F. Masters, T. Maschmeyer, A. M. Vassallo, *RSC Adv.* **2016**, *6*, 110548.
[37] M. Watanabe, M. L. Thomas, S. Zhang, K. Ueno, T. Yasuda, K. Dokko, *Chem. Rev.* **2017**, *117*, 7190.
[38] R. Kawano, M. Watanabe, *Chem. Commun.* **2005**, *16*, 2107.
[39] S. Park, D. H. Han, J. G. Lee, T. D. Chung, *Appl. Energy Mater.* **2020**, *3*, 5285.
[40] C. E. S. Côrtes, R. B. Faria, *Inorg. Chem.* **2004**, *43*, 1395.

[41] C. L. Bentley, A. M. Bond, A. F. Hollenkamp, P. J. Mahon, J. Zhang, *J. Phys. Chem. C* **2014**, *118*, 22439.
[42] I. Rubinstein, M. Bixon, E. Gileadi, *J. Phys. Chem.* **1980**, *84*, 715.
[43] I. Rubinstein, E. Gileadi, *J. Electroanal. Chem. Interfacial Electrochem.* **1980**, *108*, 191.
[44] A. Yao, F. Qu, Y. Liu, G. Qu, H. Lin, S. Hu, X. Wang, T. Chu, *Dalton Trans.* **2019**, *48*, 16249.
[45] K. Larsson, K. Binnemans, *Green Chem.* **2014**, *10*, 4595.
[46] X. Li, A. van den Bossche, T. Vander Hoogerstraete, K. Binnemans, *Chem. Commun.* **2018**, *54*, 475.
[47] A. van den Bossche, E. de Witte, W. Dehaen, K. Binnemans, *Green Chem.* **2018**, *20*, 3327.
[48] A. van den Bossche, W. Vereycken, T. Vander Hoogerstraete, W. Dehaen, K. Binnemans, *ACS Sustainable Chem. Eng.* **2019**, *7*, 14451.
[49] X. Li, Z. Li, M. Orefice, K. Binnemans, *ACS Sustainable Chem. Eng.* **2019**, *7*, 2578.
[50] A. I. Popov, D. H. Geske, *J. Am. Chem. Soc.* **1958**, *80*, 1340.
[51] A. I. Popov, D. H. Geske, *J. Am. Chem. Soc.* **1958**, *80*, 5346.
[52] A. Cerquetti, P. Longhi, T. Mussini, G. Natta, *J. Electroanal. Chem. Interfacial Electrochem.* **1969**, *20*, 411.
[53] I. G. Dioum, J. Vedel, B. Tremillon, *J. Electroanal. Chem. Interfacial Electrochem.* **1982**, *139*, 323.
[54] I. V. Nelson, R. T. Iwamoto, *J. Electroanal. Chem.* **1964**, *7*, 218.
[55] B. Bennett, J. Chang, A. J. Bard, *Electrochim. Acta* **2016**, *219*, 1.
[56] G. D. Allen, M. C. Buzzeo, C. Villagrán, C. Hardacre, R. G. Compton, *J. Electroanal. Chem.* **2005**, *575*, 311.
[57] G. D. Allen, M. C. Buzzeo, I. G. Davies, C. Villagrán, C. Hardacre, R. G. Compton, *J. Phys. Chem. B* **2004**, *108*, 16322.
[58] L. Yu, X. Jin, G. Z. Chen, *J. Electroanal. Chem.* **2013**, *688*, 371.
[59] A. P. Abbott, *ChemPhysChem* **2005**, *6*, 2502.
[60] F. A. Redeker, A. Kropman, C. Müller, S. E. Zewge, H. Beckers, B. Paulus, S. Riedel, *J. Fluorine Chem.* **2018**, *216*, 81.
[61] G. Chatel, J. F. B. Pereira, V. Debbeti, H. Wang, R. D. Rogers, *Green Chem.* **2014**, *16*, 2051.
[62] T. Iwasita, M. C. Giordano, *Electrochim. Acta* **1969**, *14*, 1045.
[63] J. G. Vos, A. Venugopal, W. A. Smith, M. T. M. Koper, *J. Electrochem. Soc.* **2020**, *167*, 46505.
[64] a) J. Cornog, E. E. Bauer, *J. Am. Chem. Soc.* **1942**, *64*, 2620; b) Y. Yagi, A. I. Popov, *Inorg. Nucl. Chem. Lett.* **1965**, *1*, 21; c) Y. Yagi, A. I. Popov, *J. Inorg. Nucl. Chem.* **1967**, *29*, 2223; d) A. Parlow, H. Hartl, *Z. Naturforsch.* **1985**, *40b*, 45; e) A. Parlow, H. Hartl, *Acta Cryst. B* **1979**, *35*, 1930.
[65] N. G. Connelly, W. E. Geiger, *Chem. Rev.* **1996**, *96*, 877.
[66] S. M. Batterjee, M. I. Marzouk, M. E. Aazab, M. A. El-Hashash, *Appl. Organomet. Chem.* **2003**, *17*, 291.
[67] E. H. B. Anari, M. Romano, W. X. Teh, J. J. Black, E. Jiang, J. Chen, T. Q. To, J. Panchompoo, L. Aldous, *Chem. Commun.* **2016**, *52*, 745.
[68] J. C. Swarts, A. Nafady, J. H. Roudebush, S. Trupia, W. E. Geiger, *Inorg. Chem.* **2009**, *48*, 2156.
[69] R. J. Enemaerke, J. Larsen, T. Skrydstrup, K. Daasbjerg, *Organometallics* **2004**, *23*, 1866.
[70] K. S. Thanthiriwatte, M. Vasiliu, D. A. Dixon, K. O. Christe, *Inorg. Chem.* **2012**, *51*, 10966.
[71] a) S. Rozen, *Adv. Synth. Catal.* **2010**, *352*, 2691; b) V. I. Sobolev, V. B. Radchenko, R. V. Ostvald, V. D. Filimonov, I. I. Zherin, *Procedia Chem.* **2014**, *11*, 88.
[72] S. I. Ivlev, A. V. Malin, A. J. Karttunen, R. V. Ostvald, F. Kraus, *J. Fluorine Chem.* **2019**, *218*, 11.
[73] M. R. Ciumag, T. Tzedakis, C. A. Barrès, *Electrochim. Acta* **2012**, *70*, 142.
[74] H. Meinert, U. Groβ, *Z. Chem.* **1969**, *9*, 190.
[75] M. F. Wempe, *J. Mol. Struct.* **2001**, *562*, 63.
[76] a) G. Gritzner, J. Kuta, *Pure Appl. Chem.* **1984**, *56*, 461; b) C. G. Zoski, *Handbook of electrochemistry*, Elsevier, Amsterdam, Oxford, **2007**.
[77] S. Mattsson, G. Senges, S. Riedel, B. Paulus, *Chem. Eur. J.* **2020**, Accepted paper.

Manuscript received: September 4, 2020
Revised manuscript received: December 11, 2020